



Development of the spectral-based dynamical core of the JMA operational global model

Masashi UJIIE¹, Daisuke HOTTA², Yukihiro KUROKI¹,
Kohei ARANAMI² and Hiromasa YOSHIMURA²

1. Numerical Prediction Division, Japan Meteorological Agency
2. Meteorological Research Institute, Japan Meteorological Agency

Contents

- Overview of operational Global Spectral Model (GSM)
- Evolution of GSM as a spectral-based dynamical core
- Recent progress of the GSM dynamical core
 - Importance of numerics, particularly “mimetic discretization”
- Research preparing for further resolution increase

OVERVIEW OF GSM

Overview of GSM (dynamical core)

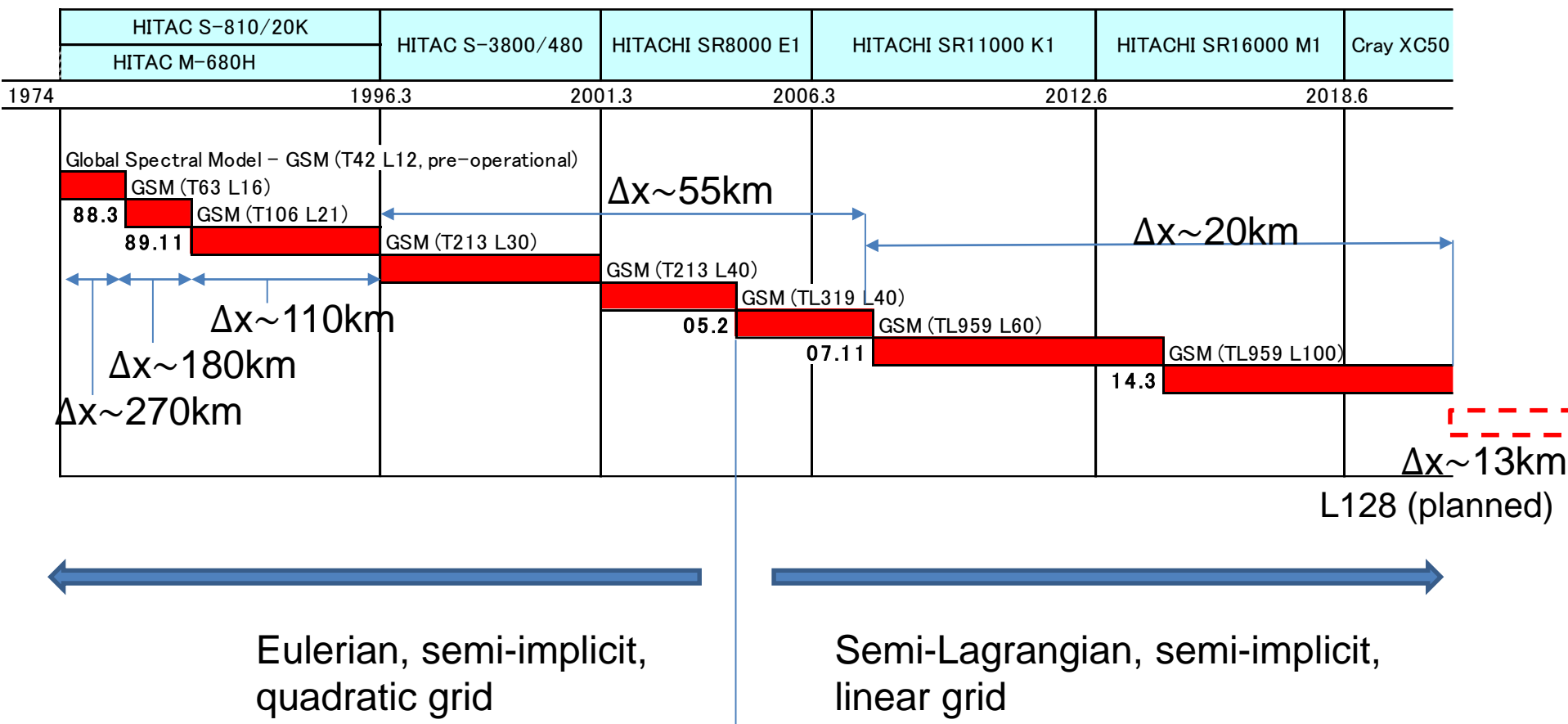
Basic formulation	Hydrostatic primitive equations (HPEs) u, v, T, Q, CWC and InPs as prognostic variables
Horizontal resolution (spectral)	TL959 (for deterministic*), approx. 20km grid spacing Reduced Gaussian grid
Vertical representation (finite difference)	Sigma-pressure hybrid coordinates 100 levels up to 0.01 hPa, based on Simmons and Burridge (1981)
Advection + Time integration	A two time level semi-implicit and semi-Lagrangian method

* TL479 (~40km) for global ensemble,
TL159 (~110km) for atmosphere-ocean coupled ensemble

For more detail, please see “OUTLINE OF THE OPERATIONAL NUMERICAL WEATHER PREDICTION AT THE JAPAN METEOROLOGICAL AGENCY”

<http://www.jma.go.jp/jma/jma-eng/jma-center/nwp/outline2019-nwp/index.htm>

History of resolution upgrade GSM (High-res. Deterministic forecast)



EVOLUTION OF GSM AS A SPECTRAL-BASED DYNAMICAL CORE

Eulerian GSM (1988--2005)

- A Hoskins and Simmons (1975) type spectral HPEs model
 - An Eulerian advection Semi-Implicit model

- Quadratic grid (following Orszag (1970)) to avoid aliasing due to advection

$$J \geq \frac{3N + 1}{2}, \quad I \geq 3N + 1$$

J : Number of latitudinal grid points

I : Number of longitudinal grid points

N : Truncation wavenumber

- Spherical harmonics as basis functions

$$A_m^n = \frac{1}{\sqrt{2\pi}} \int_{-1}^1 \int_0^{2\pi} A(\lambda, \phi) P_m^n(\mu) e^{-im\lambda} d\lambda d\mu$$

λ : longitude

ϕ : latitude

$\mu = \sin \phi$

$P_m^n(\mu)$: associated Legendre function
normalized to 1

- Divergence and vorticity as prognostic variables for momentum

- Sigma-pressure hybrid vertical coordinate (Simmons and Burridge 1981)

- Upper air (above ~60hPa): isobaric
 - Near the surface :terrain (surface pressure) following

Taking advantages of spectral methods

- Accurate calculation of horizontal gradient
 - No dispersion error
 - Accurate advection and wave propagation
 - An Eulerian shallow water model using GSM's dynamical core performs Williamson et al. (1992) 's testcase 2 with l2 error norm on the order of 10^{-14}
- Ease of solving a Helmholtz equation in spectral space

$$(\mathbf{I} - (\Delta t)^2 \mathbf{A} \nabla^2) \mathbf{D}(\lambda, \phi) = \mathbf{S}(\lambda, \phi)$$



$$\mathbf{D}_n^m = \left(\mathbf{I} + (\Delta t)^2 \frac{n(n+1)}{a^2} \mathbf{A} \right)^{-1} \mathbf{S}_n^m$$

Semi-Lagrangian GSM (2005--)

- GSM has steadily increased its resolution, but this was not achieved with increase in computing capacity alone.
 - Improvements and restructuring to numerical methods have been incorporated
 - To harness the evolving computer architecture.
 - Adaptation to massively parallel computers
 - Stable integration with a longer time stepping
- Retained the advantages of the spectral method

Introduction of a semi-Lagrangian advection scheme + linear grid

- Avoided time stepping constraint from CFL conditions

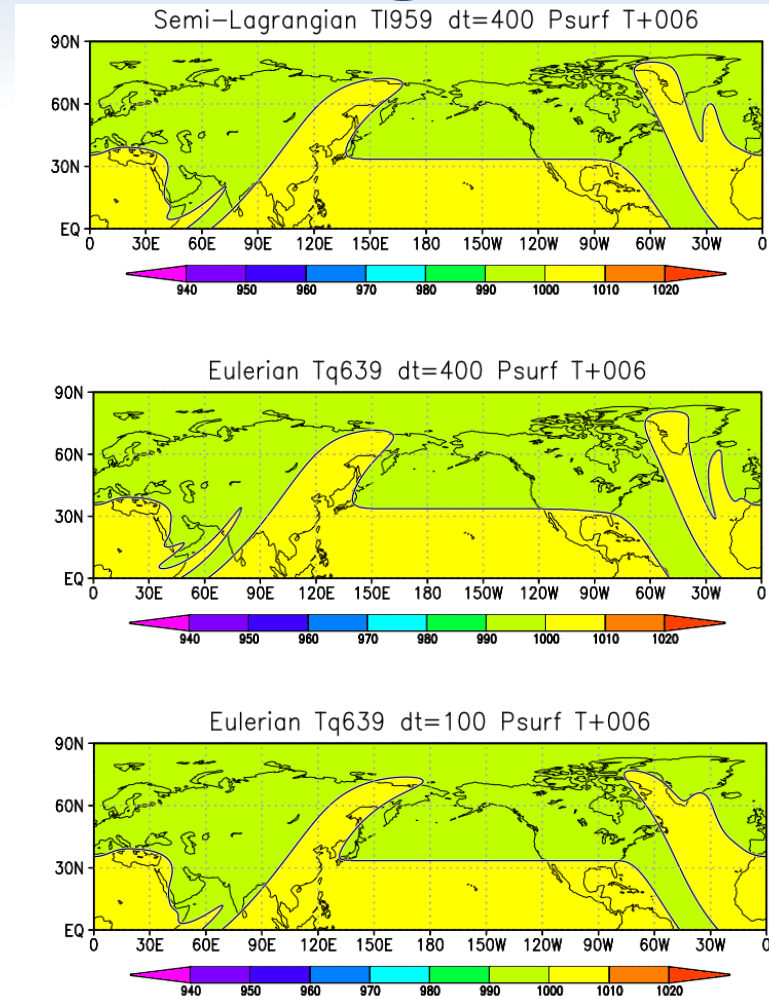
- Allowed GSM to run with Δt of 400s for TL959L100
- Linear grid for larger truncation wavenumber

$$J \geq \frac{2N + 1}{2}, \quad I \geq 2N + 1$$

- An example of importing a grid-based modelling technique to a spectral model

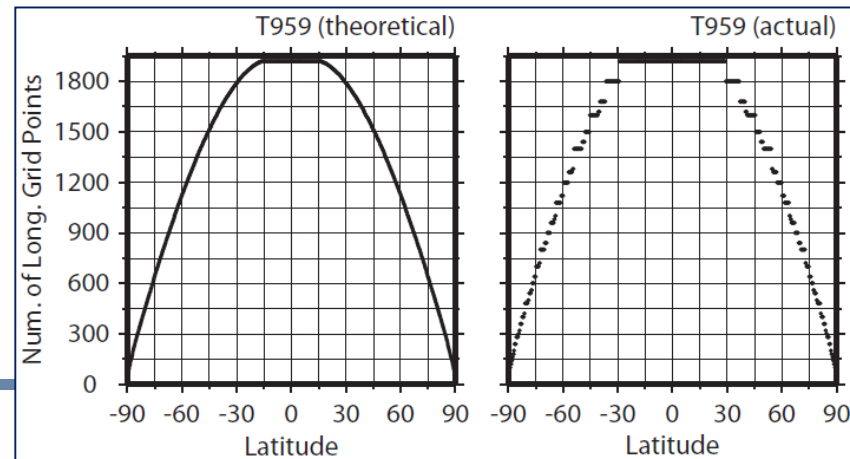
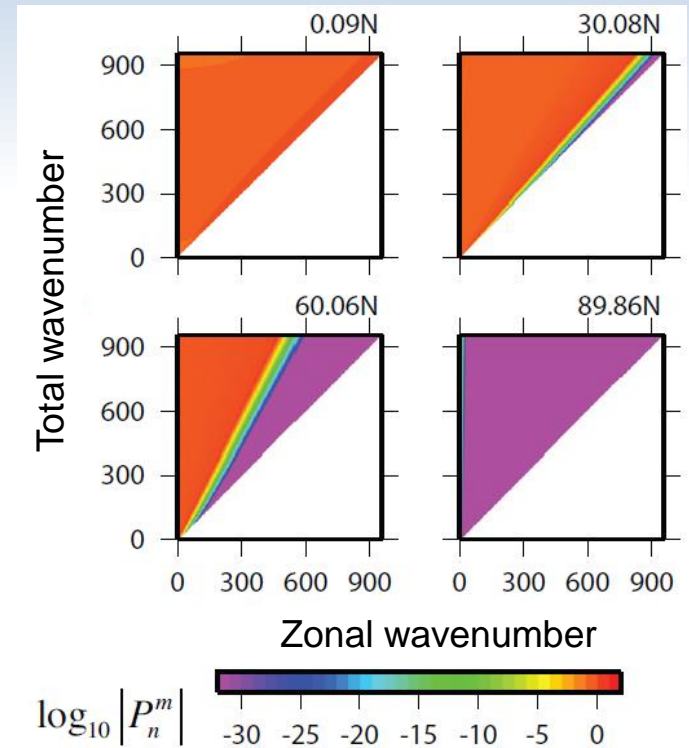
- For more detail:

- Yoshimura and Matsumura (2003)
- JMA outline 2019



Reduced spectral transforms

- The idea is based on Juang (2004)
- Implementation into GSM: Miyamoto (2006)
 - Reduced number of gridpoints and zonal wavenumber components by omitting associate Legendre functions which have negligibly small values
 - Threshold set to 10^{-16} (\sim machine epsilon of 64-bit float) to achieve exact spectral transform.
 - 28.8% reduction of the number of gridpoints in TL959



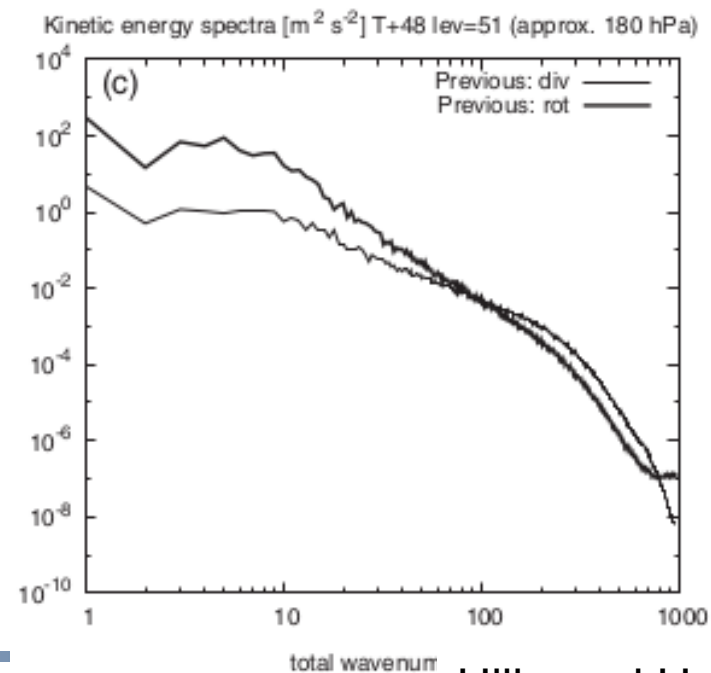
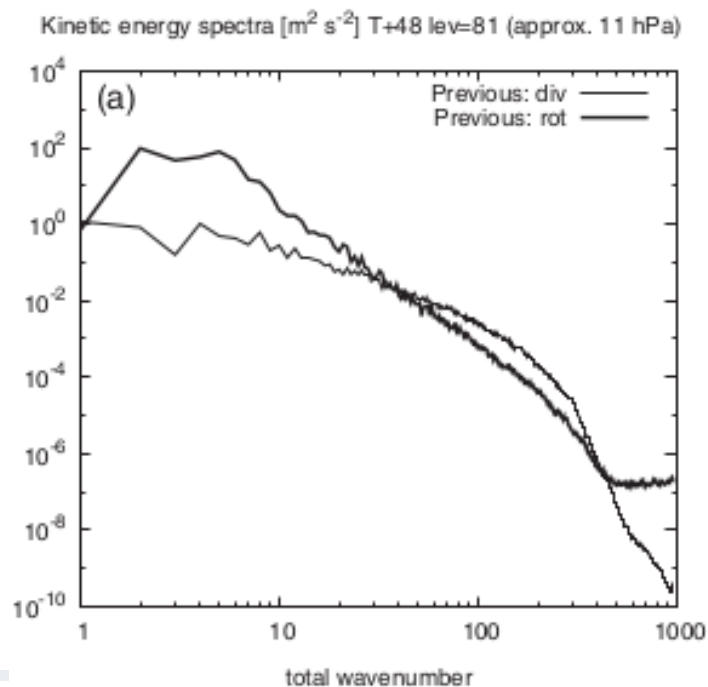
Speed up of spectral transforms

- As resolution increases, computational cost of spectral transforms become larger since
 - Computational cost is proportional to N^3
 - Bottleneck in all-to-all MPI communication
- → Speeded up calculation of the Legendre transform
 - Using cache-tuned matrix-matrix or matrix-vector libraries
 - GSM on cray XC50 employs the dzgemm routine from Intel MKL library
- Optimized MPI communication
 - Appropriate two-dimensional decompositions at each stage
 - Physics parametrization, I/O etc : XY decomposition
 - FFT: YZ decomposition
 - Legendre: ZM decomposition

RECENT PROGRESS OF THE GSM DYNAMICAL CORE DEVELOPMENT

Revisiting a “spectral blocking problem”

- The increase of horizontal resolution on the linear grid has led us to revisit the issue of spectral blocking.
- Due to aliasing from pressure gradient terms



Spectral blocking arised from pressure gradient terms

Pressure gradient force in HPEs:

$$\mathbf{F}_{\text{pgrad}} = -\nabla_p \Phi = -\nabla_\eta \Phi - R_d T_v \nabla_\eta \ln p$$

horizontal gradient of
geopotential height
on isobaric surface

horizontal gradient of
geopotential height
on eta-surface

horizontal gradient of
pressure on eta-
surface

If an eta-level is isobaric, the pressure gradient force is rotation-free as $\nabla \times \nabla = 0$.

Spectral blocking arised from pressure gradient terms

Represent the pressure gradient force as combination of $\nabla\Phi_s$, ∇T_v and $\nabla \ln p_s$ (horizontal gradients of surface orography, virtual temperature and surface pressure)

$$\begin{aligned} \mathbf{F}_{\text{pgrad},k} &= -(\nabla_p \Phi)_k = -\nabla_\eta \Phi_k - (R_d T_v \nabla_\eta \ln p)_k \\ &= \underbrace{-\nabla_\eta \Phi_s}_{(1)} + \underbrace{\sum_{l=1}^k H_{l,k}(p_s, T_v) \nabla_\eta T_{v,l}}_{(2)} + \underbrace{I_k(p_s, T_v) \nabla_\eta \ln p_s}_{(3)}. \end{aligned}$$

- The rotation free property of $\mathbf{F}_{\text{pgrad}}$ is not ensured in this discretized system even though spectral methods ensure $\nabla \times \nabla = 0$ and accurate calculation of $\nabla\Phi_s$, ∇T_v and $\nabla \ln p_s$.
 - $\nabla \times ((2) + (3)) = 0$ is not ensured.
- (2) and (3) are nonlinear w.r.t. T_v and p_s , hence the linear grid generates aliasing errors in the rotational component.
 - As resolution increases, the nonlinearity of $\mathbf{F}_{\text{pgrad}}$ also increases.

Eliminating spectral blocking that arises from pressure gradient force

- Existing remedies (as employed at ECMWF)
 - Applying de-aliasing filters
 - Employing higher order grid
 - Selective hyperdiffusion (NCEP spectral GFS)
- We proposed an alternative method which ensures rotation-free property
 - By taking advantage of spectral methods
 - Requires no parameters tuning

A new discretization method

A new discretization incorporated into the current GSM

$$\mathbf{F}_{\text{pgrad},k} = -\nabla_{\eta} \Phi_k - (R_d T_v \nabla_{\eta} \ln p)_k$$

Calculation procedures:

1. Calculate Φ_k as in Simmons and Burridge (1981)

$$\Phi_k = \Phi_s + \sum_{l=1}^{k-1} R_d T_{v,l} \ln \left(\frac{p_{l-1/2}}{p_{l+1/2}} \right) + \alpha_k R_d T_{v,k}$$

2. Calculate $\nabla \Phi_k$ in spectral space

Spectral methods ensure $\nabla \times \nabla \Phi_k = 0$

3. Calculate the second term $(R_d T_v \nabla \ln p)$ as in Simmons and Burridge (1981)

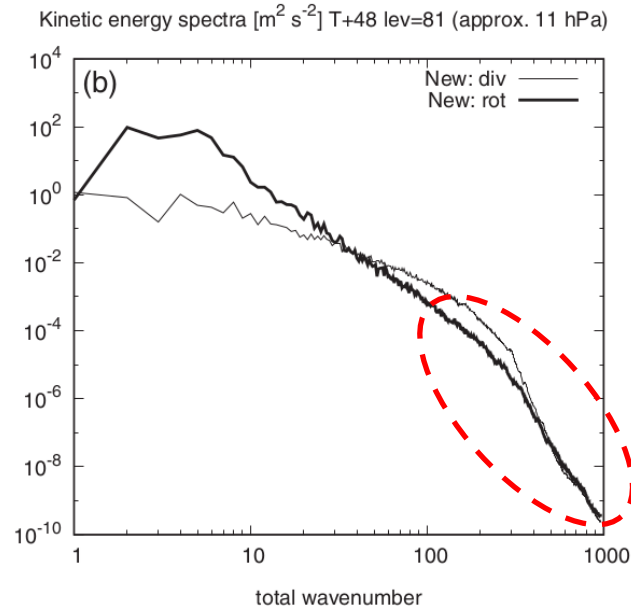
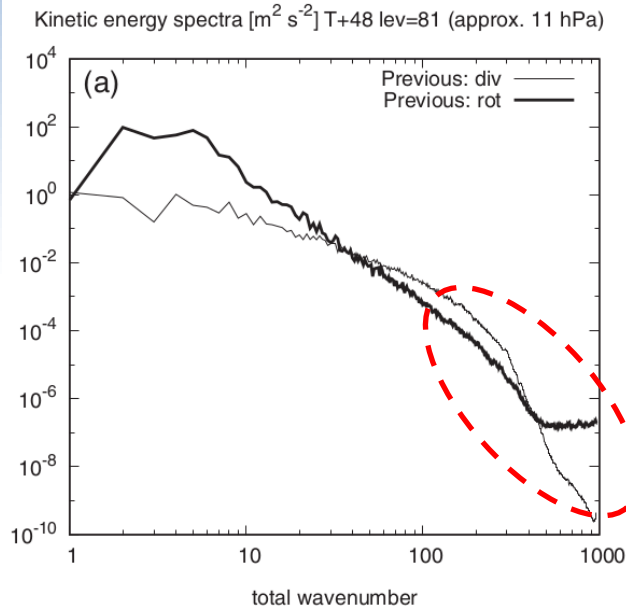
$$-(R_d T_v \nabla_{\eta} \ln p)_k = -\frac{R_d T_{v,k}}{\Delta p_k} \left[\ln \frac{p_{k-1/2}}{p_{k+1/2}} \nabla_{\eta} p_{k+1/2} + \alpha_k \nabla_{\eta} \Delta p_k \right].$$

Always zero on isobaric surface since $\nabla p = 0$

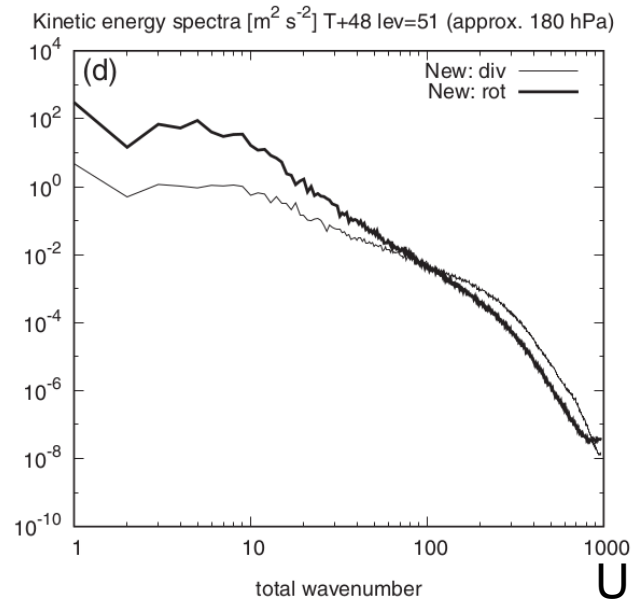
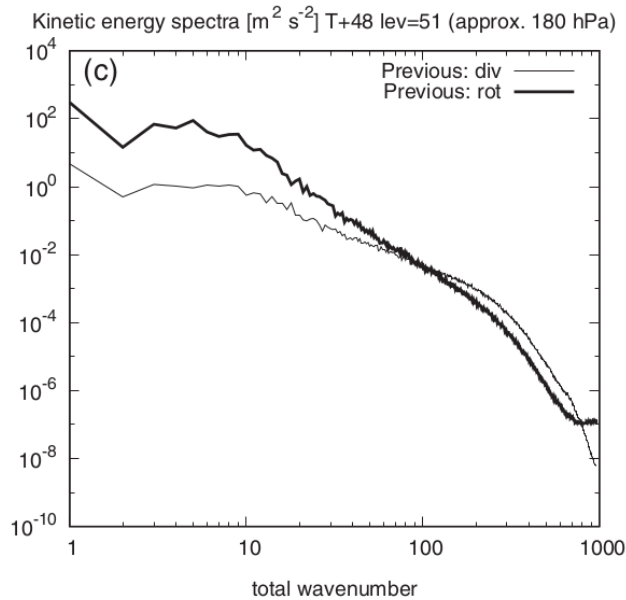
As long as we calculate horizontal gradient and rotation operators in spectral space, the rotation-free property is ensured on isobaric surface

OLD

NEW



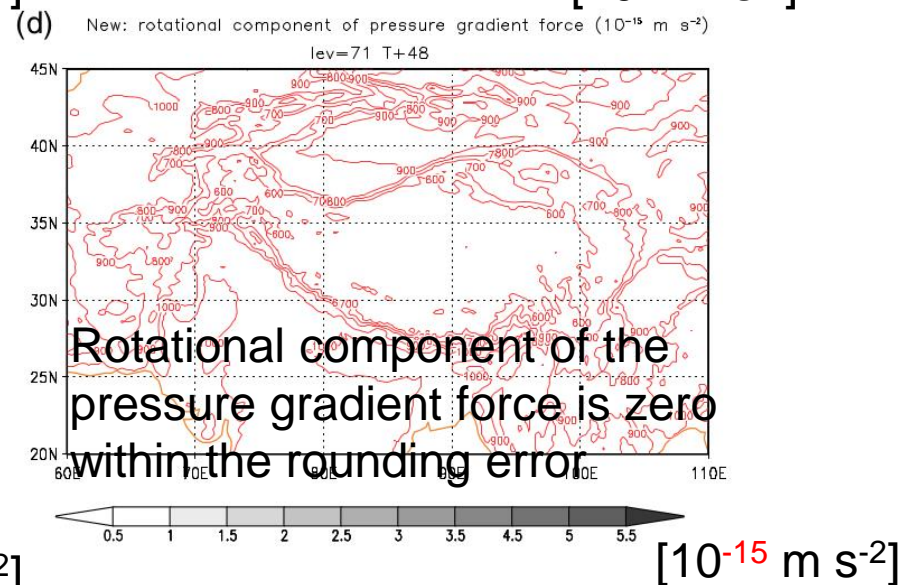
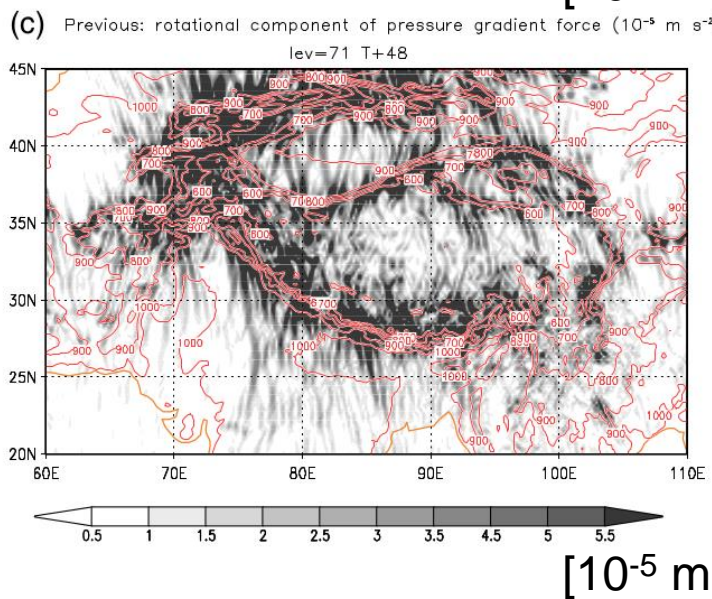
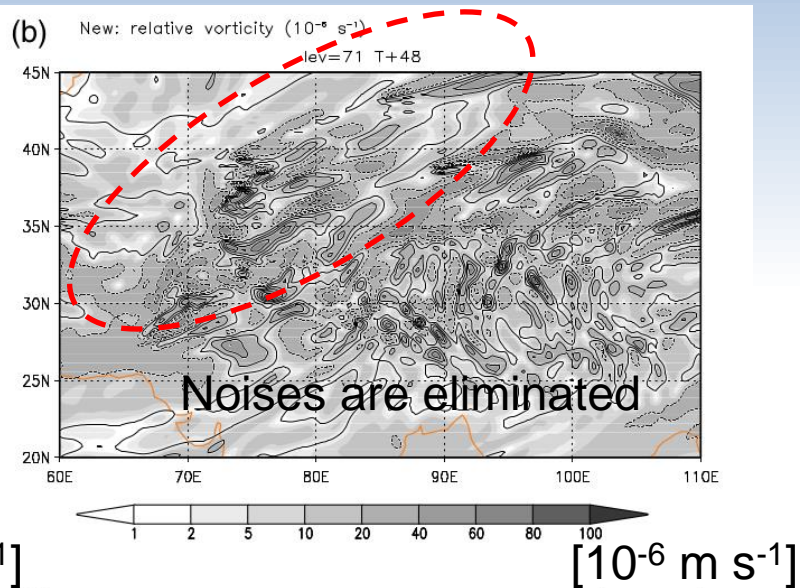
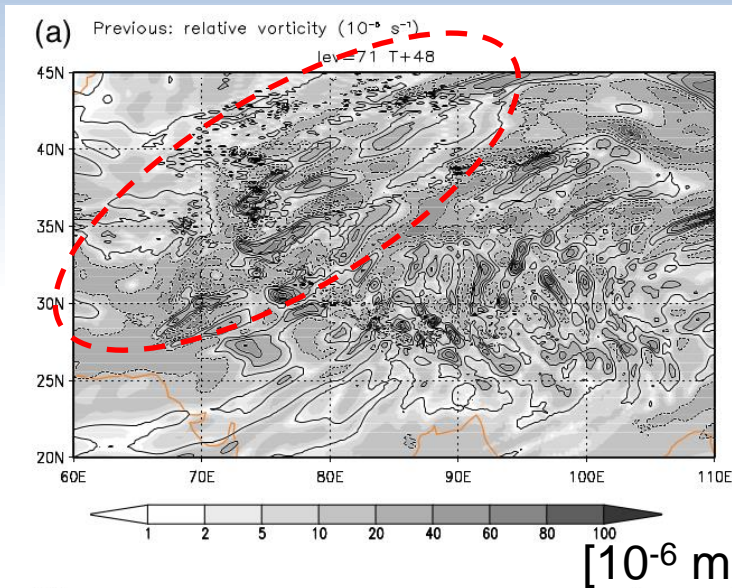
Spectral blocking is eliminated at isobaric levels



Spectral blocking still exists but smaller at the upper troposphere where eta-levels are under transition from sigma to isobaric surface.

Ujiie and Hotta (2019)

Relative vorticity (top) and rot. component of pressure gradient force (bottom) at 5hPa



Ujiie and Hotta (2019)

Lessons learned from the spectral blocking problem

- Importance of numerics, “mimetic discretization” in particular
 - keep mathematical property after discretization
 - This case implied importance of ensuring the rotation-free property of the pressure gradient terms as whole
 - In addition to ensuring $\nabla \times \nabla = 0$ operator-wise
- This will serve as a guideline for choice of the future discretization methods, no matter whether we go for spectral or grid-based method.

RESEARCH PREPARING FOR FURTHER RESOLUTION INCREASE

Toward further resolution increase

- Requires to incorporate grid-based modelling techniques for a gradual transition to spectral-grid hybridization
- Because of serious challenge in computational performance on massively parallel computers
 - Non-locality in calculating horizontal derivatives will be a bottleneck of computational performance.
 - If non-hydrostatic global models for short to medium range forecasts are necessary, (iterative) Helmholtz solvers with non-constant coefficients will be required

Research on new grid systems

- Motivation
 - Extend GSM to incorporate grid-based techniques
 - Multigrid approaches
 - Calculation of horizontal derivatives with better locality
 - Enable both accurate spectral transforms and multigrid approaches on a same grid
 - Gaussian grid is not suitable for multigrid since distribution of gridpoints with J nodes are never collocated with those of any other J' nodes
- Equispaced latitudinal grid with Clenshaw-Curtis quadrature is a promising choice
 - Hotta and Ujiie (2018)

Clenshaw-Curtis (CC) quadrature

$$X_n^m = \sum_{j=1}^J X^m(\phi_j) \tilde{P}_n^m(\sin \phi_j) w_j^{CC}$$

$$w_j^{CC} = \frac{4 \sin \theta_j}{J+1} \sum_{\substack{1 \leq p \leq J \\ p: \text{ odd}}} \frac{\sin(p\theta_j)}{p}$$

Legendre transform

$$\phi_j = \frac{\pi}{2} \left(1 - \frac{2j}{J+1} \right),$$

$$j = 1, 2, \dots, J$$

Latitudinal gridpoints

Equispaced, including the equator

$$J \geq 2N + 1 \text{ Cubic}$$

Condition for avoiding aliasing

ensured

Orthogonality/normality of P_n^m

Gauss-Legendre quadrature

$$X_n^m = \sum_{j=1}^J X^m(\phi_j) \tilde{P}_n^m(\sin \phi_j) w_j^G$$

$$w_j^G = \frac{2}{JP'_J(\sin \phi_j) P_{J-1}(\sin \phi_j)}$$

roots of $P_J(\sin \phi_j) = 0$,
 $j = 1, 2, \dots, J$

Non-equispaced, not including the equator

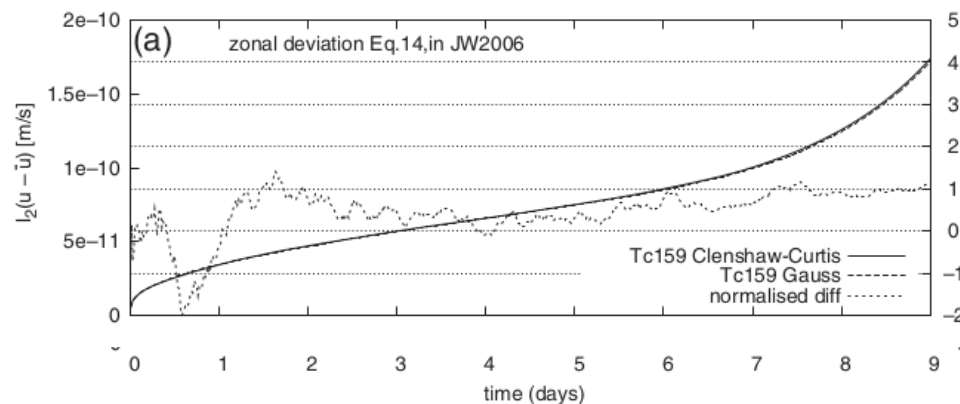
$$J \geq (2N + 1)/2 \text{ Linear}$$

ensured

- Orthogonality / normality of associate Legendre functions guarantees accurate spectral transforms
- Only minor code changes are required to implement CC grid into Gaussian grid based models.

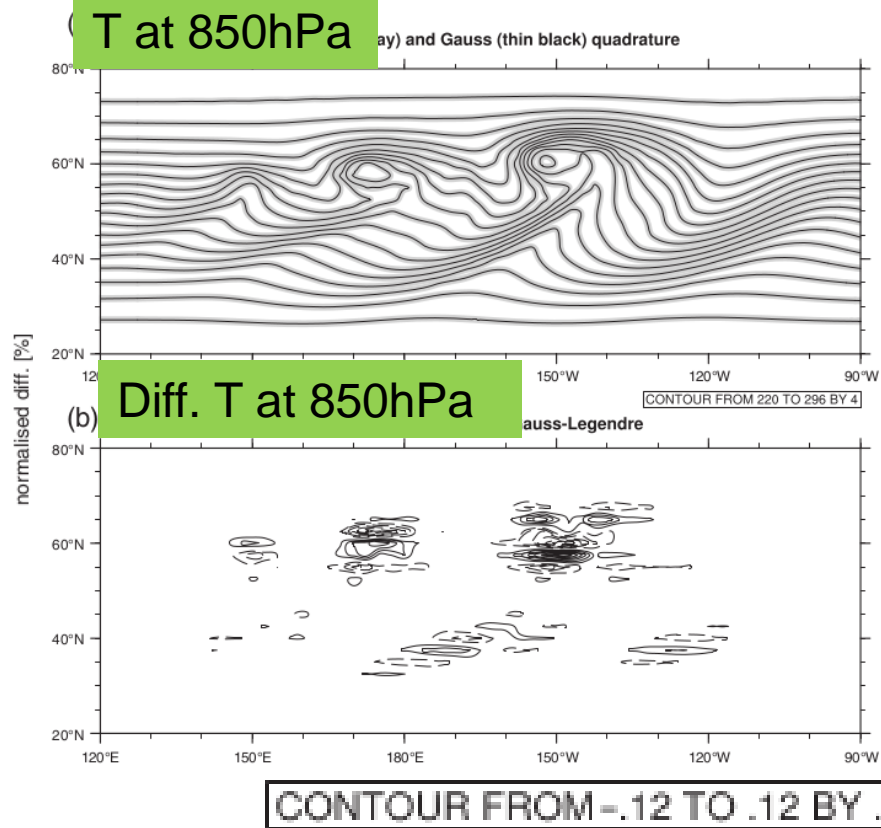
Jablonowski and Williamson (2006) tests

Steady state test



performance with CC grid is almost identical to that with Gaussian grid.

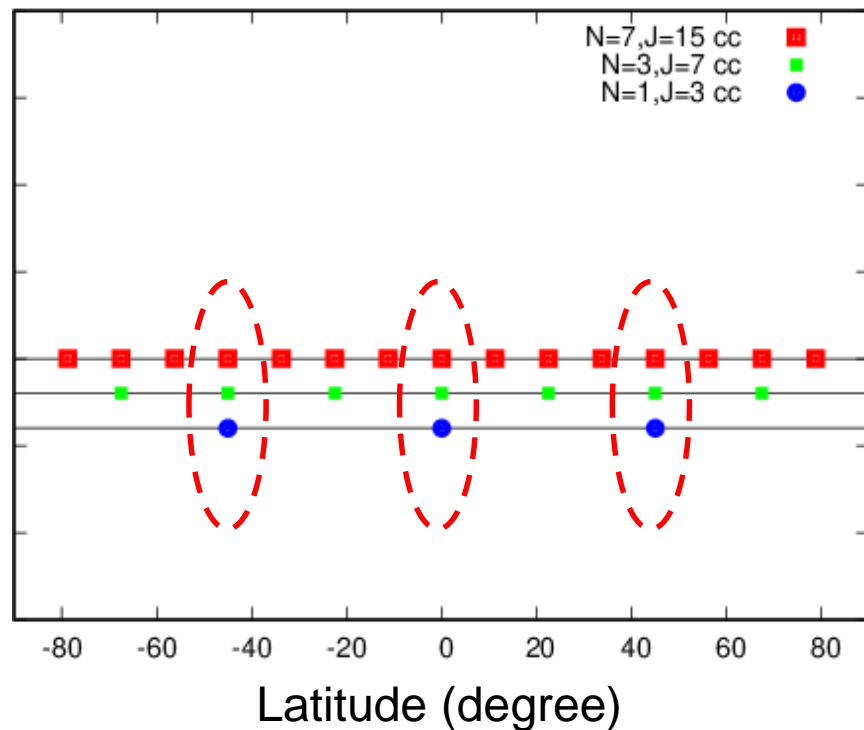
Baroclinic instability waves test



Hotta and Ujiie (2018)

A sketch on multi-grid implementation

The CC grid enables nestable grid systems e.g. (N=7,J=15) contain gridpoints those in (N=3,J=7) and (N=1, J=3)



Iterative procedures for solving a Helmholtz equation

1. Solve higher wavenumber components of D in fine grid

$$(\mathcal{I} - \mathcal{L}_f) \mathbf{D}_f = \mathbf{S} \quad \text{grid}$$

2. Restrict the residual into coarse grid (by thinning gridpoints from the fine grid)

$$\mathbf{r} = \mathbf{F}_{f2c} (\mathbf{S} - (\mathcal{I} - \mathcal{L}) \mathbf{D}_f)$$

3. Solve lower wavenumber components of error of D

$$(\mathcal{I} - \mathcal{L}_c) \Delta \mathbf{D}_c = \mathbf{r} \quad \text{grid or spectral}$$

4. Prolong the error into the fine grid and add to Df

$$\mathbf{D}_{f,\text{next}} = \mathbf{D}_f + \mathbf{F}_{c2f} (\Delta \mathbf{D}_c)$$

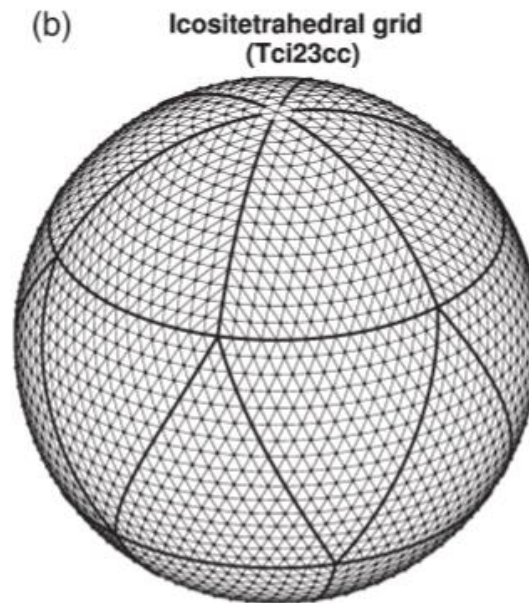
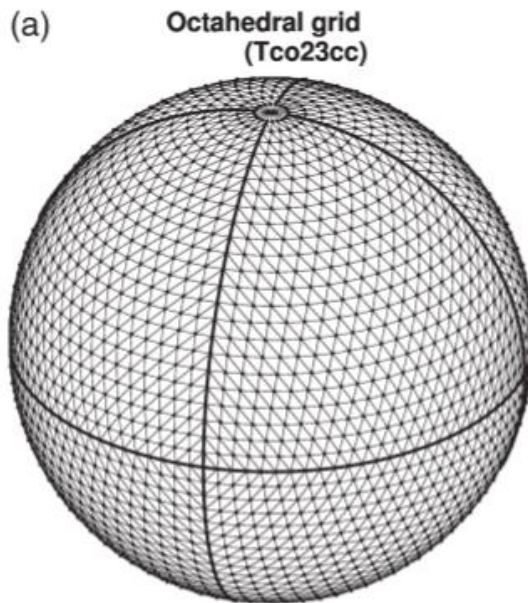
5. Check convergence of the error norm

(Repeat 1.- 5. until convergence)

Quasi-uniform grid modelling using the CC grid

Octahedral (=8-face) CC grid

Icositrahedral (=24-face) CC grid
(more compatible with Miyamoto (2006)'s reduced spectral transform rule)



Hotta and Ujiie (2018)

Research on Double Fourier Series (DFS) based global spectral model

- Another study on equispaced latitudinal grid system with Fourier transforms is ongoing
 - Computational costs are proportional to $O(N^2 \log N)$, those for Legendre transform is proportional to $O(N^3)$
- A possible choice if the cost of $O(N^3)$ computational is more problematic than communication cost
 - Also runs stably with Clenshaw-Curtis grid
- Nakano et al. (2017) conducted typhoon forecast experiments using 7km mesh nonhydrostatic DFS model and others (NICAM, MSSG)

New basis functions of the DFS model

Modified for $m > 1$ from basis functions of Cheong (2000)

$$T(\lambda, \varphi) \cong \sum_{m=-M}^M T_m(\varphi) e^{im\lambda}$$

λ : longitude

φ : colatitude

m : zonal wavenumber

n : latitudal wavenumber

M : truncation zonal wavenumber

N : truncation latitudal wavenumber

$$T_m(\varphi) \cong \begin{cases} \sum_{n=0}^N T_{n,m} \cos n\varphi & |m| = 0 \\ \sum_{n=0}^{N-1} T_{n,m} \sin \varphi \cos n\varphi & |m| = 1 \\ \sum_{n=0}^{N-2} T_{n,m} \sin^2 \varphi \cos n\varphi & |m| \geq 2, m: \text{even number} \\ \sum_{n=1}^{N-2} T_{n,m} \sin^2 \varphi \sin n\varphi & |m| \geq 3, m: \text{odd number} \end{cases}$$

These basis functions assure continuity of scalar variables and their derivatives (e.g. u and v winds) at the poles

Summary

- JMA has been operating the operational spectral model for 30 years taking advantages of spectral methods
- A number of improvements to numerical methods have been incorporated to harness the evolving computer architecture.
- Recent experience of eliminating spectral blocking let us re-recognize importance of numerics
 - “mimetic discretization” in particular
- For further high-resolution modelling, research is ongoing on new grid systems to foster gradual transition from spectral to spectral-grid hybrid approaches

References

- Hoskins, B. J. and A. J. Simmons, 1975: A multi-layer spectral model and the semi-implicit method., Quarterly Journal of the Royal Meteorological Society, 101, 637--655
- Hotta, D. and M. Ujiie, 2018: A nestable, multigrid-friendly grid on a sphere for global spectral models based on Clenshaw--Curtis quadrature, Quarterly Journal of the Royal Meteorological Society, 144, 1382-1397.
- JMA, 2019, Outline of the operational numerical weather prediction at the Japan Meteorological Agency March 2019., Appendix to WMO Technical Progress Report on the Global Data-processing and Forecasting System (GDPFS) and Numerical Weather Prediction (NWP) Research, <http://www.jma.go.jp/jma/jma-eng/jma-center/nwp/outline2019-nwp/index.htm>
- Miyamoto, K., 2006: Introduction of the Reduced Gaussian Grid into the Operational Global NWP Model atJMA. CAS/JSC WGNE Res. Activ. Atmos. Oceanic Modell.,36, 06.09-06.10.






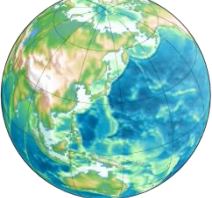
References

- Nakano and co-authors, 2017: Global 7-km mesh nonhydrostatic Model Intercomparison Project for improving TYphoon forecast (TYMIP-G7): experimental design and preliminary results , *Geosci. Model Dev.*, 10, 1363-1381
- S. A. Orszag, 1970: Transform Method for the Calculation of Vector-Coupled Sums: Application to the Spectral Form of the Vorticity Equation., *Journal of the Atmospheric Sciences*, 27, 890-895.
- Simmons, A. J. and D. M. Burridge, 1981: An Energy and Angular-Momentum Conserving Vertical Finite-Difference Scheme and Hybrid Vertical Coordinates., *Monthly Weather Review*, 109, 758-766.
- Ujiie, M. and D. Hotta, 2019: Elimination of spectral blocking by ensuring rotation-free property of discretized pressure gradient within a spectral semi-implicit semi-Lagrangian global atmospheric model., *Quarterly Journal of the Royal Meteorological Society*, 145, 3351-3358.
- Yoshimura, H. and T. Matsumura, 2003: A Semi-Lagrangian Scheme Conservative in the Vertical Direction. *CAS/JSC WGNE Res. Activ. Atmos. Oceanic Modell.*, 33, 03.19-03.20.

BACKUP SLIDES

Current NWP models in JMA

In Operation

	In Operation					
	Global Spectral Model GSM	Meso-Scale Model MSM	Local Forecast Model LFM	Global Ensemble GEPS	Meso-scale Ensemble MEPS	Seasonal Ensemble CPS2
objectives	Short- and Medium-range forecast	Disaster reduction Aviation forecast	Aviation forecast Disaster reduction	One-week forecast Typhoon forecast Early warning on extreme weather One-month forecast	Disaster reduction Aviation forecast	Seasonal forecast (three month forecast, cold/warm season outlook) El Nino outlook
Forecast domain	Global 	Japan and its surroundings (4080km x 3300km) 	Japan and its surroundings (3160km x 2600km) 	Global 	Japan and its surroundings (4080km x 3300km) 	Coupled Global Atmosphere and Ocean 
Horizontal resolution	TL959 (0.1875 deg)	5km	2km	TL479 / TL319 (0.375 / 0.5625 deg)	5km	Atmos.: 1.125 deg Ocean:0.3-0.5x1 deg
Vertical levels / Top	100 0.01 hPa	76 21.8km	58 20.2km	100 0.01 hPa	76 21.8km	Atmos.: 60 (~0.1 hPa) Ocean: 52 with BBL* *Bottom Boundary Layer
Forecast Hours (Initial time)	132 hours (00, 06, 18 UTC) 264 hours (12 UTC)	51 hours (00, 12 UTC) 39 hours (03, 06, 09, 15, 18, 21 UTC)	10 hours (00-23 UTC hourly)	264 h (00, 12 UTC) 132 h (06, 18 UTC)* 27 members Extend to 432 h (4times/week) 816 h (4times/week) 13 members	39hours (00,06,12,18 UTC) 21 members	210 days (00UTC) 51 members / month
Initial Condition	Global Analysis (Hybrid 4D-Var)	Meso-scale Analysis (4D-Var)	Local Analysis (3D-Var)	Global Analysis with ensemble perturbations (SV, LETKF)	Meso-scale Analysis with ensemble perturbations (SV)	JRA-55 with ensemble perturbations (BGM)

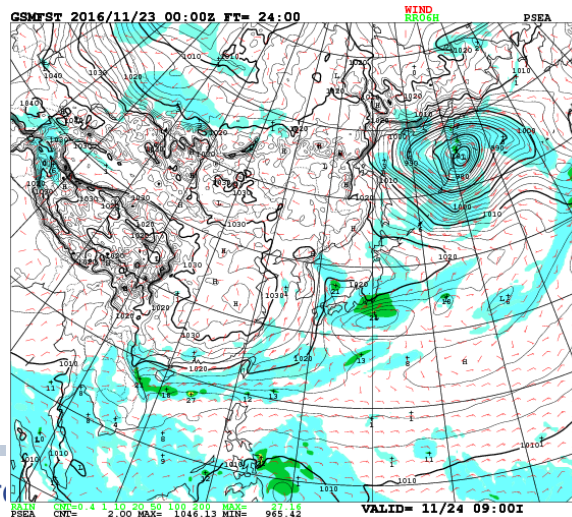
* when a TC of TS intensity or higher is present or expected in the RSMC Tokyo - Typhoon Center's area of responsibility (0°–60°N, 100°E–180°). 35

Overview of GSM (parameterization schemes)

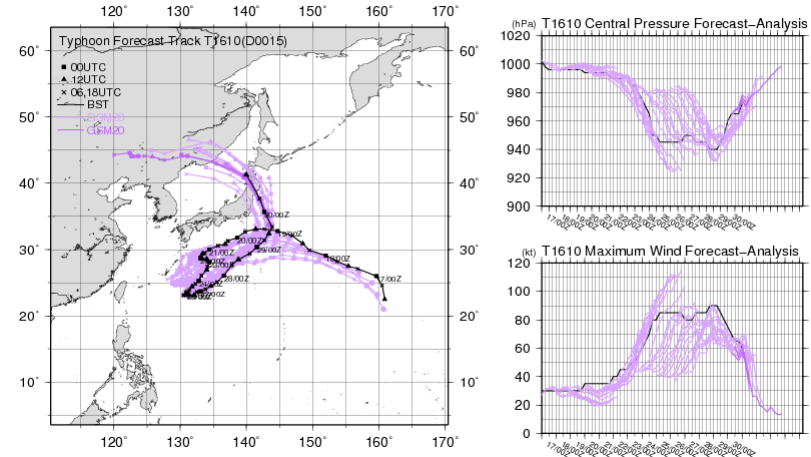
Convection	A spectral-type mass flux scheme based on Arakawa-Schubert (1974) considering ice phase and very simple micro physics
Cloud	A PDF-based condensation scheme based on Smith (1990) with simplified microphysics such as conversion of precipitation from cloud condensate, evaporation and snow melting. A cloud ice and snow fall scheme is also included.
Boundary layer	A kind of Mellor Yamada level 2 scheme (+ diffusive coefficients defined by Han and Pan (2011) for stable BL)
Surface exchange coefficients	Using the Monin-Obukhov's similarity law (Beljaars and Holtslag, 1991)
Radiation	Two stream absorption approximation (long wave) Two stream δ -Eddington approximation (short wave)
Land surface	An improved Simple Biosphere (SiB) model
Subgrid Gravity waves	Orographic ($o(100\text{ km})$): Palmer et al. 1986 Orographic ($o(1-10\text{ km})$): Iwasaki et al. 1989 Non-orographic: Scinocca 2003

Roles of GSM as the operational model

- GSM provides:
 - basic information for short- and medium-range, one week, one month and seasonal forecasts
 - basic information for typhoon track and intensity forecasts
 - first guess of the operational global data assimilation system
 - Older versions of GSM are used in the JRA-25 and JRA-55 reanalyses
 - lateral and upper boundary conditions for the operational Meso-Scale Model
 - etc



T1610(D0015) Typhoon Forecast and Analysis (Track and Intensity)

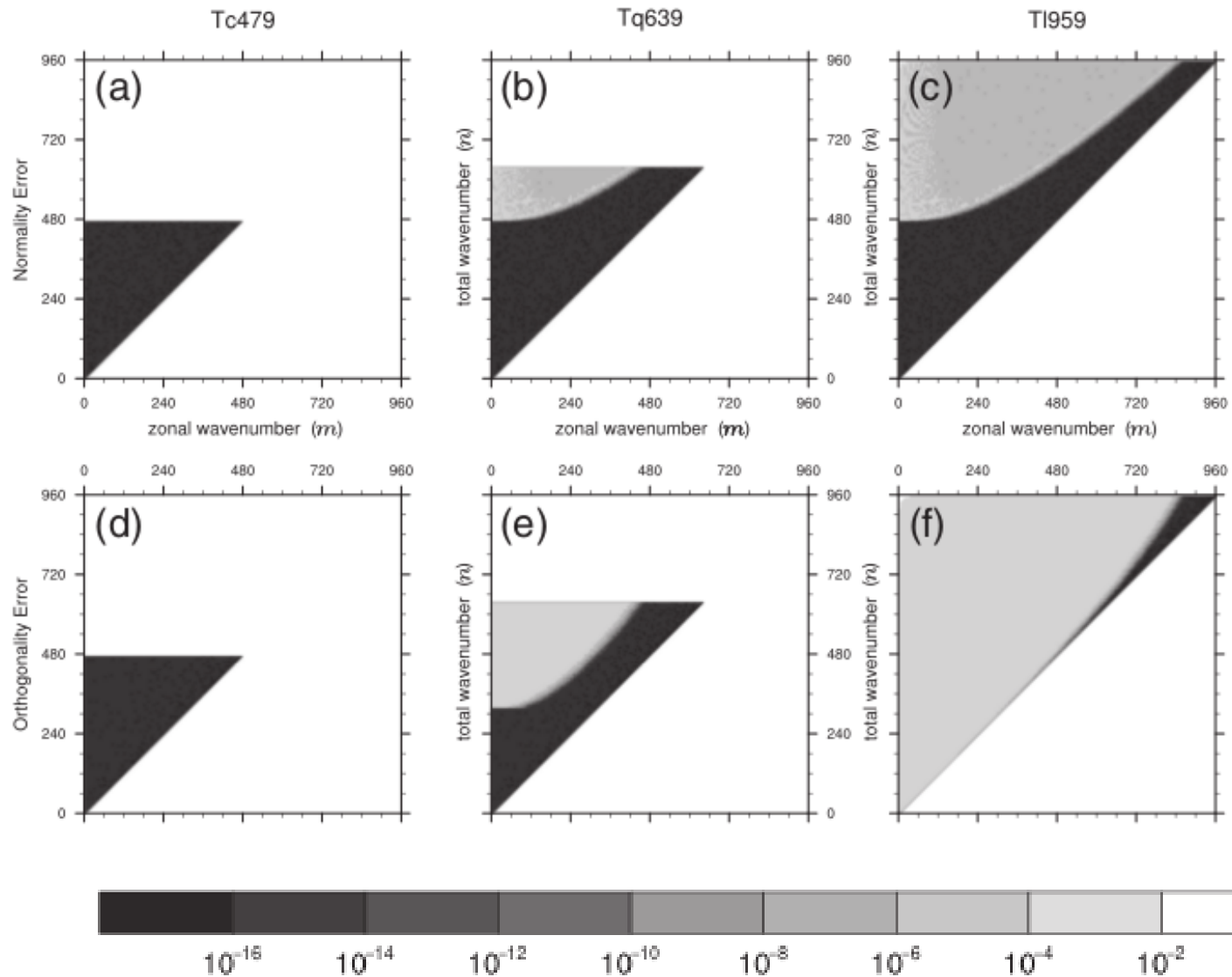


History of resolution upgrade GSM

Versions of GSM GSM\$YY\$MM \$YY: last two digits of year MM: month	Resolution T\${X} \${N} L \${L} X: grid type N : truncation wavenumber L : number of vertical levels	HPC upgrade
GSM8803	Tq63L16 (up to 10 hPa)	Mar. 1988
GSM8911	Tq106L21 (up to 10 hPa)	
GSM9603	Tq213L30 (up to 10 hPa)	Mar. 1996
GSM0103	Tq213L40 up to 0.4 hPa	
GSM0503	TI319L40 up to 0.4 hPa	Mar. 2001
GSM0711	TI959L60 up to 0.1hPa	Mar. 2006
GSM1403	TI959L100 up to 0.01hPa	Jun. 2012
GSM21XX (planned)	TI959L128 up to 0.01hPa	Jun. 2018
GSM22XX (planned)	TI1279L128 or Tq959L128 up to 0.01hPa	

HU18

Normality and orthogonality error of CC quadrature



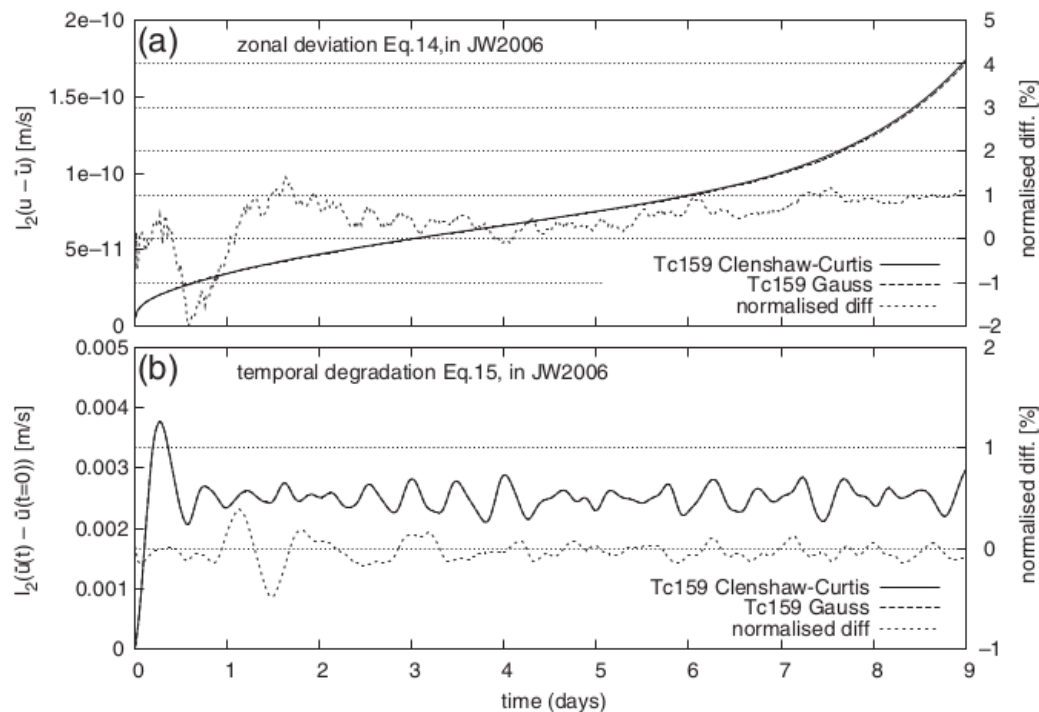


FIGURE 5 l_2 measures of steady-state maintenance in the steady-state test of Jablonowski and Williamson (2006) computed for Clenshaw–Curtis (solid) and Gaussian (dashed) versions of the dynamical core of JMA-GSM. (a) the zonal symmetry measure $l_2 \{u(t) - \bar{u}(t)\}$. (b) the temporal degradation of the zonal mean zonal wind $l_2 \{\bar{u}(t) - \bar{u}(t = 0)\}$. Note that the solid and dashed lines are almost superposed in both (a) and (b). The dotted lines (to be read on the right axis) represent the relative difference between the Clenshaw–Curtis and Gaussian results normalized by the values of Gaussian results

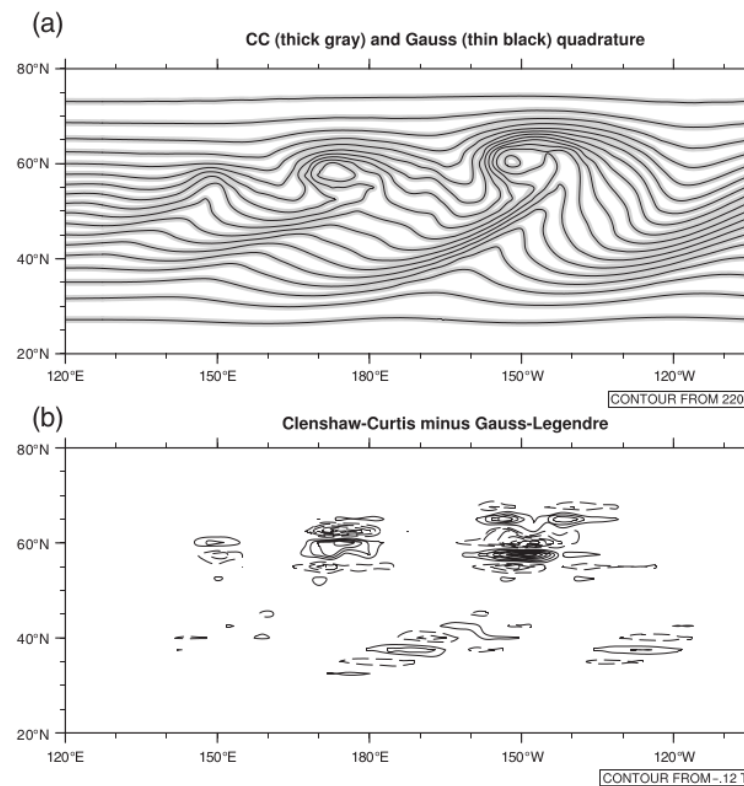
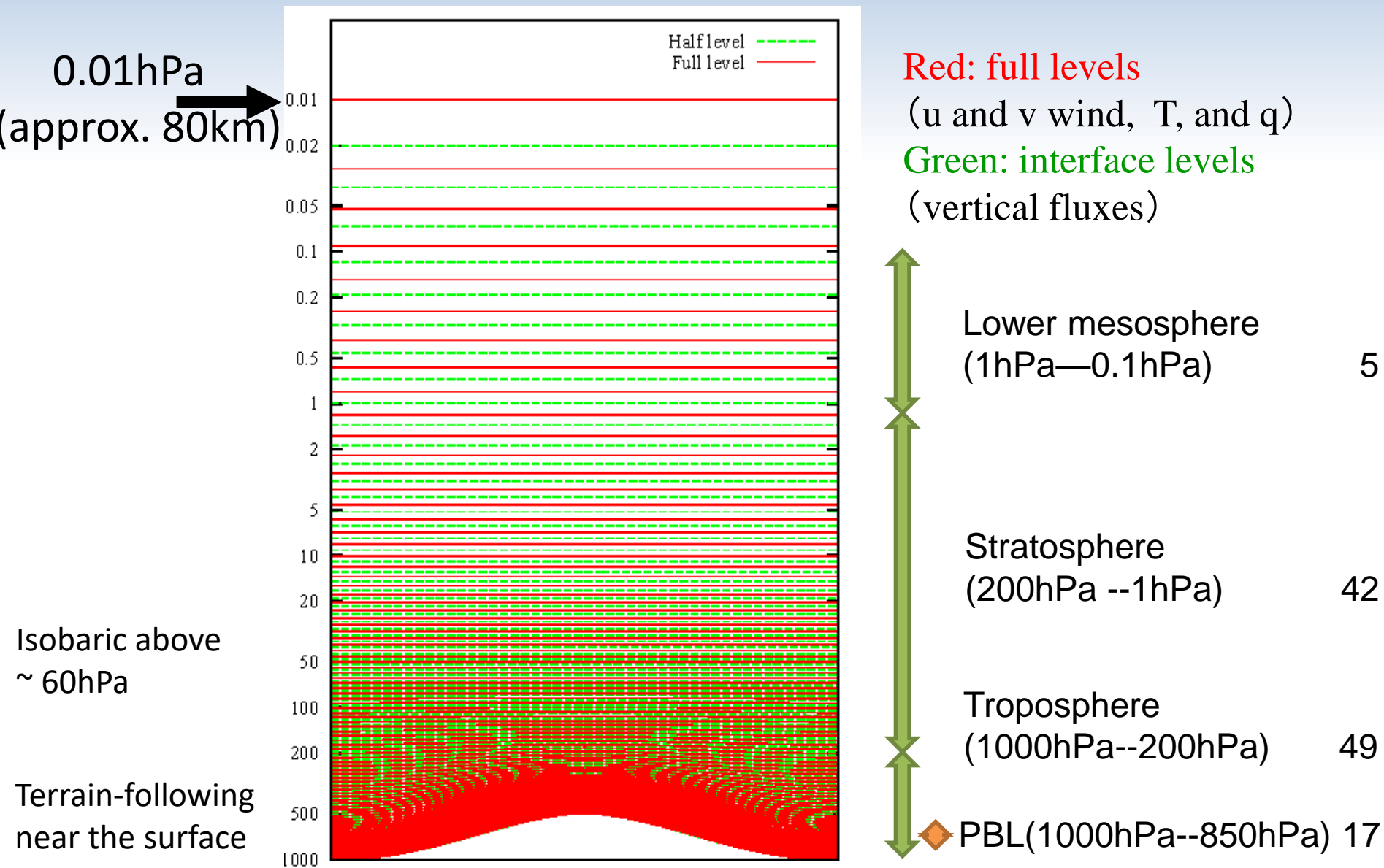
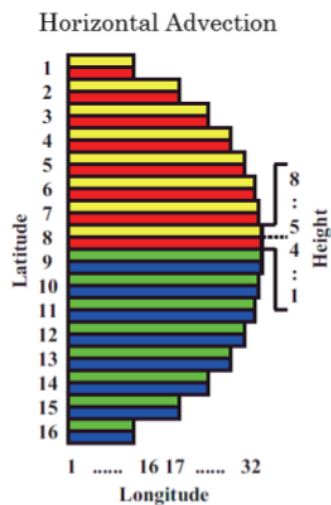
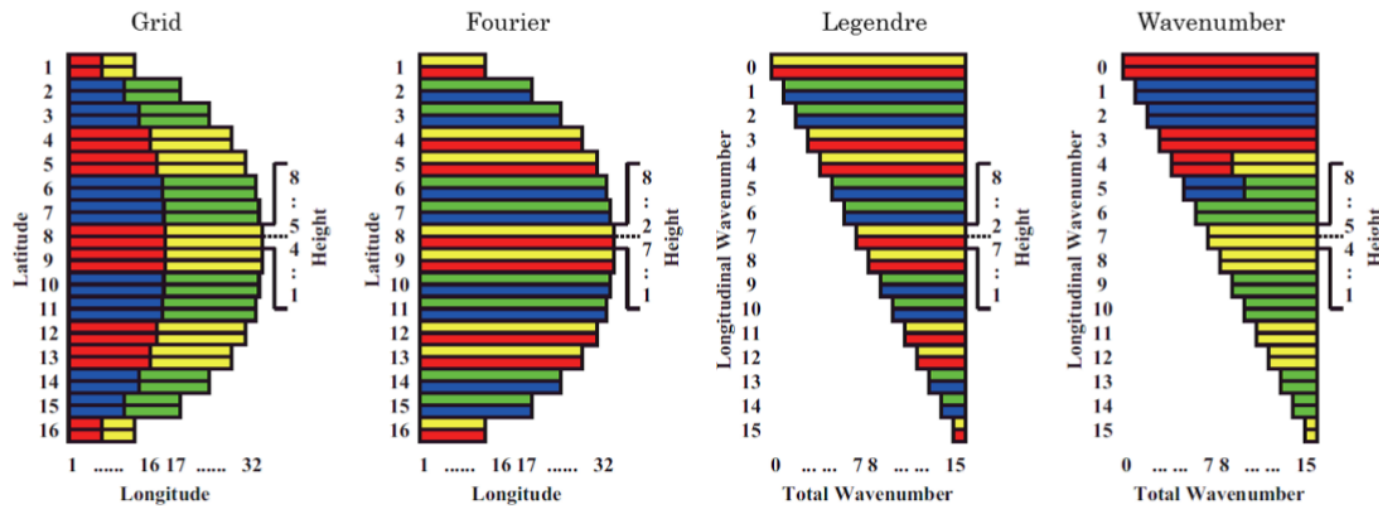


FIGURE 6 (a) Snapshot of 850 hPa temperature at day 9 from the baroclinic instability wave test case produced with Clenshaw–Curtis (thick gray lines) and Gaussian (thin black lines) versions of JMA-GSM dynamical core run at Tc159 resolution, and (b) the difference between the two. Contour intervals are 4 K in (a) and 0.02 K in (b). In (b), positive values are drawn with solid contours and negative values with dashed contours. Note that in (a) the two sets of contours are completely superimposed

Vertical coordinate in GSM (100 levels up to 0.01 hPa)





stage	purpose
Grid (base)	physics parameterization, nonlinear terms in the dynamical process, and I/O
Fourier	FFT
Legendre	Legendre transform
Wavenumber	solving a Helmholtz equation and horizontal diffusion in the spectral space
Horizontal Advection	Semi-Lagrangian advection

JMA(2019)

Figure 3.2.4: Schematic design of the parallelization. The number of processes used is assumed to be 4 in this example. Colors in the figure represent the rank for the computation in that area; red is rank 0, yellow is rank 1, blue is rank 2 and green is rank 3.

UH19

Why spectral blocking is so undesirable?

- It contaminates signals by noises
- It can be source of computational instabilities
- It violates the principle that assures accuracy of spectral methods
 - “As wavenumber is larger, the spectral coefficient is asymptotically converged to zero.”

DFS

Performance on the former supercomputer at MRI, JMA

On Fujitsu FX100 120nodes 240MPI processes

TL1919L100 (10km)
72 hours forecast

